ROYAL SOCIETY OF CHEMISTRY

PAPER

Check for updates

Aging of living polymer networks: a model with patchy particles

Stefano Iubini, [ID] *[ab] Marco Baiesi[bc] and Enzo Orlandini[bc]

Microrheology experiments show that viscoelastic media composed by wormlike micellar networks display complex relaxations lasting seconds even at the scale of micrometers. By mapping a model of patchy colloids with suitable mesoscopic elementary motifs to a system of worm-like micelles, we are able to simulate its relaxation dynamics, upon a thermal quench, spanning many decades, from microseconds up to tens of seconds. After mapping the model to real units and to experimental scission energies, we show that the relaxation process develops through a sequence of non-local and energetically challenging arrangements. These adjustments remove undesired structures formed as a temporary energetic solution for stabilizing the thermodynamically unstable free caps of the network. We claim that the observed scale-free nature of this stagnant process may complicate the correct quantification of experimentally relevant time scales as the Weissenberg number.

1 Introduction

Many soft materials with important industrial and medical applications are formed by thermodynamic self-assembly of elementary constituents dispersed in aqueous solution.[1] This process gives rise to networks of linear or branched fibers or even more complex objects[2] that can continuously break, rejoin or get entangled. These "living" materials[3] have remarkable viscoelastic properties that are typically studied either by imposing a shear stress with a rheometer[1,4] or by dragging a micro-sized probe through the medium as in active micro-rheology.[5,6] The response and relaxation dynamics of living polymers are the result of large-scale reorientation and mutual reptation of the fibers that, in turn, depend on small scales mechanisms such as scission and rewiring of branches. This multiscale process can give rise to global relaxation dynamics that, for systems as wormlike micelles, has been measured to be of the order of seconds.[5,6]

An important issue is the relation between the macroscopic dynamical response of the system, measured experimentally, and its less accessible local structural rearrangements. From the theoretical side, mean-field theories and microscopic constitutive models have been successfully developed[3,7–10] to rationalize the outcomes of rheological experiments. However, these studies often dealt with small temperature jumps, which

may not lead to the significant disturbance of the micellar networks as, *e.g.*, in microrheological experiments at large Weissenberg numbers where a microbead is moved in the medium at high velocities.[11,12] At the same time, numerical studies,[13–18] performed at a coarse-grained molecular level on specific systems (cationic cylindrical micelles and cetyltrimethyl-ammonium chloride micelles) have either looked at the competition between shear flow and internal network dynamics or estimated the strands scission and branching free energies of these systems. However, these models, being still quite detailed and system-specific, cannot have access to the scales spanned by rheological experiments (of the order of seconds and above μm^3) or address universal features of the phenomenon.

A generic understanding of the transient behavior of living polymers can be sought by addressing the following questions: which are the dominant local structures (or "microstates") that compete dynamically in the rearrangement of a relaxing living random network? How does the long-time relaxation depend on the mechanisms of local rewiring and scission of the fibers? Is the time dependence of relevant observables undergoing relaxation characterized by simple exponentials or is it more similar to a dynamical scaling with power laws? Simulations of coarse grained models at mesoscopic level are an ideal tool for answering these questions: they allow a direct investigation both at short/small and long/large scales and they may adopt a well controlled protocol for driving the system out of equilibrium.

In this paper, we introduce a simple, coarse-grained, description of a thermally driven self-assembly process generating a living network of fibers by means of the merging, scission and rewiring of basic units that represent a portion of

[a] Consiglio Nazionale delle Ricerche, Istituto dei Sistemi Complessi, via Madonna del Piano 10, I-50019 Sesto Fiorentino, Italy. E-mail: stefano.iubini@fi.isc.cnr.it
[b] Dipartimento di Fisica e Astronomia, Università di Padova, Via Marzolo 8, I-35131 Padova, Italy
[c] INFN, Sezione di Padova, Via Marzolo 8, I-35131 Padova, Italy

Paper

the tubular structure. These units are described by patchy particles.[19–33]

By using large-scale Brownian dynamic simulations and analytical arguments to estimate the free-energy barriers between the competing "microstates", we characterize the underlying microscopic dynamics that leads to the global relaxation towards the formation of the random networks. To go beyond the regime of small perturbations a wide temperature quench is imposed on the system.

The paper is organized as follows. In Section 2 we introduce the coarse-grained model and the numerical set-up. In Section 3 we analyze the thermodynamic and kinetic properties of local motifs and their effect on the large-scale relaxation dynamics of the system upon a temperature quench towards a self-assembled equilibrium state. Section 4 is devoted to a final discussion of the results and to highlight future developments that can be explored within this approach. Finally, the appendix contains the details of the numerical methods employed for this study.

2 Model

The coarse grained model we consider belongs to the vast class of patchy particle models used in literature to study self-assembled structures[19] but it is specifically designed to describe living polymer networks and particularly worm-like micelles. Let us first introduce its basic properties in the context of patchy colloids (Section 2.1) and later discuss a more specific connection with micellar systems (Section 2.2).

2.1 Patchy colloids

The elementary unit of our coarse-grained description is a rigid body consisting of three sub-units: there is a central core of radius R (red spheres in Fig. 1(a)) and two radially opposite (i.e., antipodal) "patches" or "sticky spots" (blue transparent spheres) fixed at distance λR. The effective interaction between units is the sum of two contributions: a steric (excluded volume) interaction between the core beads and a mutual attraction between patches belonging to different rigid bodies. The first is accounted for a shifted and truncated Lennard-Jones potential with characteristic amplitude ε and range R. Patch–patch attraction, that would lead to the aggregation of units at sufficiently low temperatures, is instead described by a truncated Gaussian potential with range $\sigma = 0.4R$ and amplitude $A = 40\varepsilon$ (this amplitude allows to recover free energies at $T \approx 1$ that are comparable to the ones measured in micellar systems), see Appendix A for more details.

Two main characterizing aspects of our model are worth noticing. First, in most of the patchy colloids models[19] the branching points of the assembled structures are generated either by introducing a fraction of colloids decorated by three or more attractive patches[20,21] or by allowing for different types of patch–patch interactions.[22–25] In either case, a better control of the phase diagram is achieved by satisfying a single-bond-per-patch condition.[26] In our model only bifunctional patchy beads are considered and the local branching emerges naturally from the formation of multiple contacts between patchy particles. Note that similar systems were studied experimentally[27] and
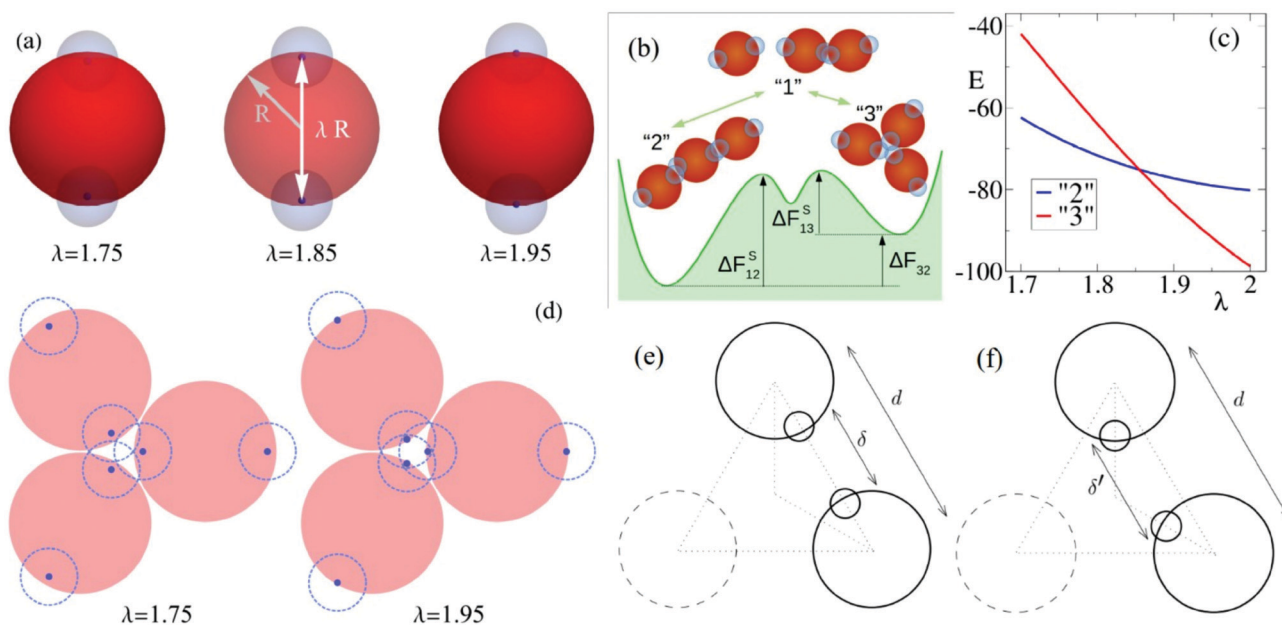
Fig. 1 (a) Example of three patchy particles: two sticky spots of range σ (light blue spheres of radius σ with darker dot at their center) form a rigid body with a (red) repulsive core of radius R. The sticky spot centers are at distance λR from each other. (b) Sketch of a possible free energy landscape for a trimer, i.e., a system with three patchy particles/micellar units. (c) Ground-state energy of linear-trimer ("2" state, blue) and branching-point ("3" state, red) configurations as a function of the branching parameter λ. (d) Sketch of a triple contact for $\lambda = 1.75$ (sticky spots farther than the interaction range σ) and for $\lambda = 1.95$ (sticky spots closer than σ). (e) and (f): geometrical details of the (planar) linear and branched configurations. The total potential energy of a strand is $E_l = 2u_l$ due to a full overlap of the sticky spots while, in a branching point, the same quantity is $E_b = 3u_b$ with a bond energy $|u_b| < |u_l|$ which tends to u_t only when λ is sufficiently large.

numerically[28–30] (see also some more recent work[31–33]). The second aspect concerns the presence of the tunable branching parameter λ. This has been introduced to mimick the propensity of worm-like micelles to branch as a function of salt concentration (see Section 2.2). In particular, by varying $\lambda \leq 2$ ($\lambda = 2$ corresponds to standard surface interactions between patches), one can change the depth of the sticky spots within the repulsive core and hence bias the system towards the formation of either linear strands or branches (see Fig. 1(b) for the simplest case of trimers). More precisely, for large values of λ the units tend to form "vertex" or "3 contact" states (see Fig. 1(b)) rather than the "strands" or "2 contact" states.

This behavior can be explained quantitatively by minimizing analytically the total potential energy of the vertex and strand configurations of a trimer, see Fig. 1(c). As a matter of fact, we find that the formation of strands is energetically advantageous with respect to branch points only for sufficiently small values of λ. Branch points become instead energetically more convenient if λ gets close enough to 2. For example, in the two situations represented in Fig. 1(d), for $\lambda = 1.75$ the mutual attraction between sticky spots take place at a distance larger than the interaction range σ, reducing the stability of the trimer, while for $\lambda = 1.95$ the three pairs of sticky spots are all at a distance within σ and thus very stable.

The effect of the branching parameter λ can be further rationalized as follows. Let us focus on a linear dimer (see Fig. 1(e)) in its mechanical equilibrium position with bond energy $u_1 < 0$ determined by the distance d between unit centers and the distance $\delta = d - \lambda$ between sticky centers. The branched configuration can be obtained by rotating the two reference units by angles of $30°$ with respect to their centers on the plain containing the trimer (Fig. 1(f)). In this rotated configuration the two sticky spots increase their distance $\delta' > \delta$ thus decreasing their attracting force, while the repulsive centers of the units are not modified significantly. Since $\delta' > \delta$ the single bond energy $u_b > u_1$. However, due to the different number of bonds in branched and linear trimers, the overall energy of the branched trimer $E_b = 3u_b$ can be lower and thus more stable than the linear trimer configuration with energy $E_1 = 2u_1$. This takes place if λ is large enough to keep δ' within the range of attraction of the sticky spots. Upon decreasing λ, one meets a situation in which δ' is longer than the range of attraction between sticky spots and hence the branched configuration becomes less stable than the linear one.

2.2 Wormlike micelles

The patchy colloid model described above is rather generic but it can be specialised on worm-like micelles for which a wealth of experimental data is nowadays available. In this context, it is known that the spatial organization of micelles in spherical, linear or branched structures depends on several parameters such as salt concentration[3,16] or the spontaneous curvature of surfactants.[34,35] This feature makes large-scale numerical simulations rather challenging, even at coarse-grained level, since a detailed description of micelles recombination
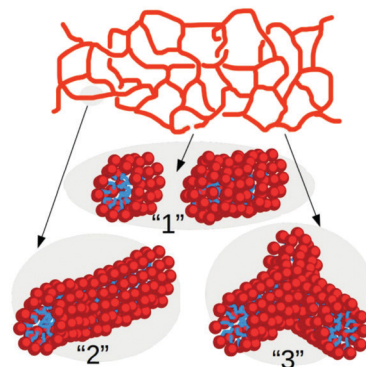

Fig. 2 Sketch of a wormlike micellar network and of selected portions where each surfactant is depicted as a hydrophilic (red) head and a hydrophobic (blue) tail. The numbering of the network portions follows that of the corresponding patchy particle states of Fig. 1(b).

dynamics requires to resolve the mutual interaction of solvent, salt and surfactant particles at the subnanometric length scales.[16,18] In contrast, in our minimal model the effect of ionic particles and curvature is taken into account effectively through the tunable branching parameter λ.

In this approach an ensemble of surfactants forming a globular micelle or the segment of a wormlike network, as those sketched in Fig. 2, is mapped to a single micellar unit. In this context, one may think of λ as a parameter describing the strength of salt concentration. This is indeed known to shrink the effective size of the hydrophilic heads of the surfactants, thus favoring the appearance of structures with negative surface curvature as hubs in the micellar network.

Note that the resolution of our coarse grained model cannot describe effects below the size of a globular micelle. In particular, unlike previous models,[13–18] the dynamics of a single surfactant is not included in our description. On the other hand, the fact that the basic element of our model is not representing a single surfactant but rather a collection (i.e., some dozens) of them, should not affect the large scale dynamics of the network structure that we aim to explore here.

2.3 Simulations

The dynamics of the system follows a set of coupled Langevin equations for the interacting units in an implicit solvent at fixed volume and constant temperature T (henceforth measured in units of ε, with Boltzmann constant $k_B = 1$ and $\varepsilon = 1$). Numerical simulations are performed with LAMMPS engine.[36] For a more detailed description of the model and for a mapping of the simulation units to those of a wormlike micellar system, see the appendix.

By assuming, for instance, that the core radius of the elementary unit length is of the order of the average width measured in wormlike micelles, i.e., $R \approx 5$ nm, the largest box considered in our simulations with dimensions $108R \times 108R \times 324R$ maps to a system volume ≈ 0.5 μm³. Moreover, our runs simulate systems of up to $N = 6000$ units; this would correspond to a number of molecules of surfactants of the order of 10^5.[37]

Finally, since the simulation time unit τ is mapped to 2 μs in the real system (see appendix), the longest simulation time we can reach, $t = 10^7\tau$, corresponds approximately to 20 s and is comparable with the duration of recent experiments.[6,38] Simulations are performed with an integration time step equal to $10^{-2}\tau$. We have verified that this time step suffices to ensure suitable numerical accuracy in all regimes considered in this study.

We describe the time evolution of the network by monitoring the formation/disappearance of its local motifs, such as dangling ends and branched structures. These are classified by looking at the number of contacts shared by their patches. A sticky spot is defined to share a contact with another one if the distance between their centers is $\leq R$, see appendix for further details. A dangling end contains a unit with $k = 1$ contacts, while each branch "3" contains three units each with $k = 3$ contacts, when they are part of a strand in the network (that is, a chain of elementary units with $k = 2$) which ends either with dangling ends or branching points. Finally, we define the length L of a strand as the total number of linear bonds between its extrema. For example, a dimer composed of two units with $k = 1$ has length $L = 1$, while a sequence on five units with $k = 2$ between two joints has length $L = 6$. We assign $L = 0$ to isolated units ($k = 0$).

3 Results

3.1 Thermodynamics and scission time of local motifs

We first analyze the equilibrium thermodynamics of the smallest motifs assembled in the network, namely the strands and the branch points (respectively state "2" and "3" in Fig. 1(b)). In presence of thermal fluctuations, the zero-temperature scenario of Fig. 1(c) is modified by entropic contributions and a comparison between the free energies F of the microstates "2" and "3" must be performed. Note that in micellar solutions thermal fluctuations not only determine the configurational entropy of the motifs, but also modify the typical energies of

strand and branch points.[35] At our coarse-graining level, this would result to a branching parameter λ that depends also on temperature. In this study, however, since we are interested in identifying the role of purely entropic contributions, T and λ are tuned independently. On the other hand, once the model is fully characterized, any mapping to a given experimental condition of salt concentration and temperature can be obtained through a suitable selection of the λ and T values.

To estimate the free energy difference $\Delta F_{32} = F_3 - F_2$ we have carried out Langevin simulations with parallel tempering sampling technique[39,40] on a system with three units confined within a small fixed volume (see appendix for details). In Fig. 3(a) we report ΔF_{32} as a function of T for four values of λ. It displays a linear growth with T, with an intercept at $T = 0$ that matches quite well the energy differences found analytically from Fig. 1(c), see open symbols. Entropy differences ΔS_{32} are thereby identified by the (negative) slope $\partial \Delta F_{32}/\partial T$, see dashed lines. Note that the combination of the negative entropy gap ΔS_{32} with a λ-dependent energy potential may result in a situation where the most favorable thermodynamic state is T-dependent, as for $\lambda = 1.95$, where branch points are stable only at low T. Analogous results involving temperature-dependent effective valence were previously found in particles models with explicit dissimilar patches.[23] These findings match the prediction[18] that wormlike micelles may form networks with a variety of features, depending on the inclination of their tubular structures to branch.

To see how local thermodynamic properties affect the dynamics of network formation, we have computed the average scission time either from the strand "2" or from the branch point "3" to the detached dimer-plus-monomer state "1", see Fig. 1(b). Scission times have been computed from equilibrium simulations for different temperatures T and different values of the branching parameter λ, see appendix for details. They follow a standard Arrhenius law once reported as a function of $1/T$. For branched initial configurations (Fig. 3(b)), we find average scission times $t_3 \sim \exp(\Delta E_{13}^S/T)$ with energy ΔE_{13}^S whose fitted values are $\Delta E_{13}^S \approx 15, 21, 26, 37$ (in units of $k_B T$),
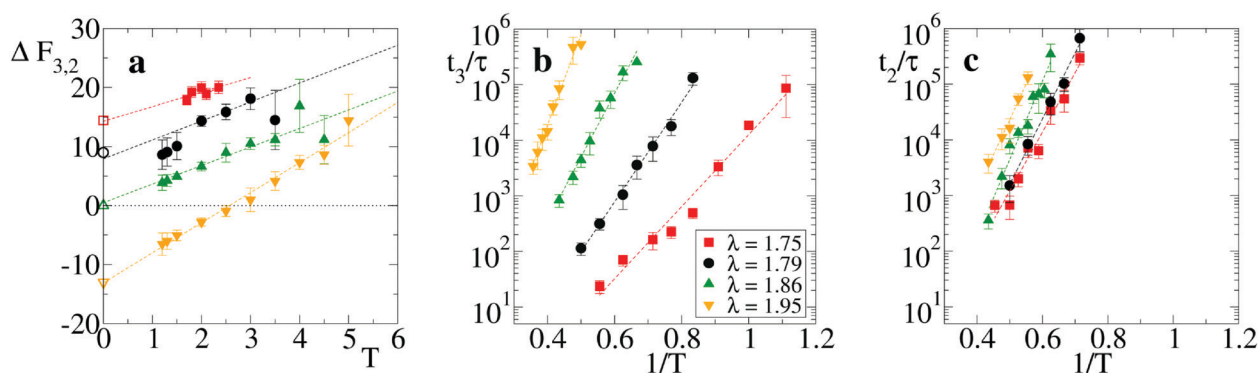
Fig. 3 Thermodynamic and kinetic properties of a trimer. (a) Free energy difference ΔF_{32} vs. temperature T for λ = 1.75, 1.79, 1.86 and 1.95. For the same values, $-\Delta S_{32}$ = 2.4, 3.2, 3.2 and 5.1 from linear fits, see dashed lines. Open symbols reported on the vertical axis correspond to the energy difference from Fig. 1(c), at T = 0. (b) Average scission time t_3 for a trimer initially arranged in the configuration "3" and (c) average scission time t_2 for a strand "2", as a function of the inverse temperature $1/T$. Dashed lines are Arrhenius fits of ΔE_{13}^S and ΔE_{12}^S. In all panels different symbols refer to different values of the branching parameter λ (see legend in panel (b)).

respectively for λ = 1.75, 1.79, 1.86, and 1.95. Similarly, the scission times for strand initial configurations is $t_2 \sim \exp(\Delta E_{12}^S/T)$ (Fig. 3(c)) and the fitted values of the scission energies ΔE_{12}^S are 24, 27, 32, and 29 for the same λ values. Importantly, these values of ΔE_{12}^S and ΔE_{13}^S are in a range $\approx$15–35 $k_B T$ fully compatible with the current estimates of the scission energies (or enthalpies) of micellar systems.[18,38,41,42]

3.2 Relaxation dynamics

Once clarified the equilibrium and kinetic properties of the basic units of the model, we now turn to the main topic of this work, namely the study of the long time relaxation process of the system towards relatively large networks at equilibrium. This is carried out by large-scale simulations in which the system starts from a solution of freely diffusing globular micelles (which in our model are represented by isolated units and initialised with $T \gg 1$). At sufficiently low T, isolated units start to aggregate into intricate networks, see the inset of Fig. 4 and 6(b). Their typical structures bear a strong resemblance of those appearing on smaller scales in less coarse-grained models.[13–18] In Fig. 4 we report the time evolution of the mean strand length $\langle L \rangle$ for λ = 1.75, T = 1 and N = 6000, where the symbol $\langle \cdot \rangle$ indicates the average over all strands found in the system at time t. Note that, for the chosen values of λ and T, equilibrium thermodynamics predicts a large predominance of strands over branching points, see red squares in Fig. 3(a). Hence the system is expected to arrange itself in long strands. However, after a relatively fast power-law growth for a time $t_0 \sim 10^3\tau$, $\langle L \rangle$ reaches first a plateau that lasts for a decade (see cyan band, whose width is $\tau_s \sim 10^4\tau$) and then slowly increases as a second power law towards the expected equilibrium value

(orange band). From numerical fits, we have found that the exponent of the two power-laws is $\simeq$1, see dashed lines in Fig. 4. The intermediate plateau on τ_s indicates that the growth of the network cannot be described in terms of a simple coalescence process,[43,44] due to the presence of a metastable state characterized by an excess of branching points (see top-left inset in Fig. 4). As a result, longer strands can be progressively assembled by slow rearrangements of the whole structure.

The macroscopic relaxation process is further understood by looking at the dynamical evolution of units classified by their contacts. Let N_k be the number of units with k contacts and $f_k = N_k/N$ their fraction. Due to the core repulsion, for $\lambda \lesssim 2$ a unit may establish at most k = 4 contacts (two per side).

In Fig. 5 we plot the fractions f_k vs time for the same system of Fig. 4. After a quick condensation to a network ($f_0 \to 0$ for $t \to t_0$), the network does not contain the equilibrium proportion of network motifs. The fraction f_1 of units at dangling ends tends slowly to zero, with a scaling compatible with a power law $f_1 \sim t^{-1}$. Eventually, at $t_{eq} \approx 2 \times 10^6\tau$, mapped to $\approx$10 s, the fraction f_1 reaches its asymptotic value. This very slow reduction of the number of strands with dangling ends highlights a stagnant global relaxation of the network. Also the fraction f_3 of units meeting at branches slowly decreases as $f_3 \sim t^{-1}$ till t_{eq} and then fluctuates around its equilibrium value. We can approximate the asymptotic ratio $\bar{f}_3/\bar{f}_2 \simeq \bar{f}_3$ (the bar over f_k denotes the long-time value of f_k) by the equilibrium expression $\bar{f}_3/\bar{f}_2 = \exp(-\Delta f_{32}/T)$, where $\Delta f_{32} = \Delta F_{32}/3$ is the free energy difference per unit derived from the single trimer problem, see Section 3.1. For λ = 1.75 and T = 1, this gives $\bar{f}_3/\bar{f}_2 \simeq 0.003$. This prediction, however, is not fully quantitative, as it neglects the role of trimer interactions (and even more complex many-body interactions) which are present in the macroscopic system. Finally, a very small amount of units with four contacts (k = 4) is temporarily observed during the relaxation process, in correspondence of the maximum concentration of branches f_3. This is not surprising, as four-contacts states arise when the branched geometry affects both sides of a unit.
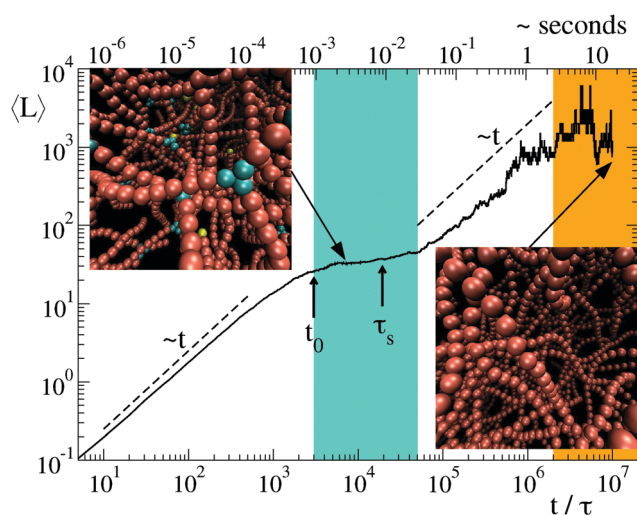

Fig. 4 Evolution of the average strand length $\langle L \rangle$ for a system of N = 6000 particles with λ = 1.75, and T = 1 (thick black curve). The cyan band marks the metastable regime with excess of branches (see an example in the upper inset) while the orange band identifies the regime of thermodynamic equilibrium (lower inset). Vertical arrows indicate the condensation time scale $t_0 \simeq 3 \times 10^3\tau \approx 1$ ms and the typical time $\tau_s \simeq 2 \times 10^4\tau$ of network rearrangements. In the two configurations of the network, units with k = 1, 2, 3 contacts are drawn, respectively, in yellow, red and cyan.
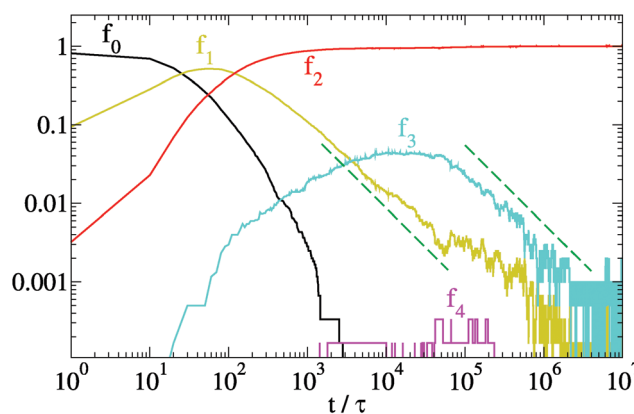

Fig. 5 Evolution of the relative density f_k of units with k-contacts for the same relaxation dynamics of Fig. 4 (N = 6000, λ = 1.75 and T = 1). Dashed lines represent a scaling $\sim t^{-1}$.

Since their energetic cost is essentially twice the cost of a single branch, their asymptotic concentration is expected to be of the order of $(\bar{f}_3)^2$, a behaviour which, however, was not observed in our simulations due to finite size and finite time effects.

The slow scalings of f_1, f_3, and $\langle L \rangle$ suggest that the dynamics within the network proceeds through a sequence of frustrated rearrangements. For instance, a dangling end joining its free cap to the side of a strand would form a branch. This local state is however thermodynamically less favorable (see Fig. 1(b)), thus leading to a subsequent decay back to a dangling end and a linear strand. A direct merging of two dangling ends would better stabilize the system but this event becomes more and more unlikely with time due to the concomitant decreases of the dangling ends population. From this argument it follows that the time scale of network rearrangements τ_s in Fig. 4 is determined by the scission time of branch points. Indeed from Fig. 3(b) we find that $t_3 \simeq 10^4 \simeq \tau_s$ for $\lambda = 1.75$ and $T = 1$.

The variety of micellar structures depends on several parameters (solvent, salt concentration, surfactant chemistry) and includes networks rich in branches. This situation is realized in our model by increasing λ. For example, with $\lambda = 2$ and $T = 1$, the relaxation proceeds through the formation of a metastable network with relatively small average strand length, as shown in Fig. 6(a) (the configuration at the end of the simulation is shown in Fig. 6(b)). Again, there is a very slow convergence of the fraction f_1 of units at the caps of dangling ends, see Fig. 6(c). In Fig. 6(d), in linear scale on the vertical axis, it is apparent that also the fractions f_2 and f_3 are slowly converging toward their asymptotic average values. Here, equilibrium thermodynamics predicts a clear dominance of branches over strands: in the single trimer study in Fig. 3(a), we obtain
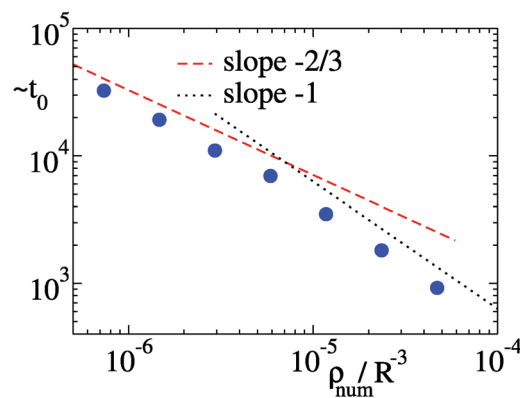

Fig. 7 Time scale of the network condensation as a function of the particle density. The straight lines indicate the scalings expected at low and high densities. Data refer to system sizes N = 25, 50, 100, 200, 400, 800, 1600, T = 1 and λ = 1.8. Particles are evolved in a cubic box with side equal to $324R$ and periodic boundary conditions.

$\Delta F_{32} \simeq -8$ for the nearby parameters λ = 1.95 and T = 1. Therefore, we conclude that equilibrium is far from being reached and that the configuration reported in Fig. 6(b) is still a metastable one.

The phenomenology described above holds for several particle densities. Indeed, by changing considerably N and keeping the volume V fixed, we have been able to vary $\rho_{num} = N/V$ by a factor of 3 (data not shown) Yet, the scaling of the mean quantities is quite similar to the previous cases. In particular, the average strand length in the initial metastable network is unaffected by the change of density. However, the density determines the time scale t_0 of the initial network condensation. This is defined as the time needed for the fraction of 0-contacts f_0 to go below the threshold value $f^* = 0.4$ starting from a homogeneous initial condition of isolated particles ($f_0 = 1$) at time $t = 0$. By scaling arguments, at low concentrations, diffusion leads to $t_0 \sim \rho_{num}^{-2/3}$. At higher concentrations it is rather the "ballistic" expansion of the network core (as in other Brownian coagulation systems[45]) that determines the time scale $t_0 \sim \rho_{num}^{-1}$. In Fig. 7 we report estimates of $\sim t_0$ (up to a constant that is irrelevant for the scaling) which are compatible with the two regimes, see also the appendix for further details. Note that we have verified that f^* is irrelevant for the scaling behavior of t_0 with ρ_{num} in so far as f^* is large enough to provide a sampling of the initial relaxation stages.

4 Discussion

We have introduced a patchy particle model to study the relaxation dynamics of living polymer networks driven out equilibrium by a deep thermal quench. A novel relevant feature of this coarse-grained description is its ability to bridge the short time dynamics of its elementary motifs (dangling ends, linear strands, branches) with the long time behavior of the mesoscopic network.
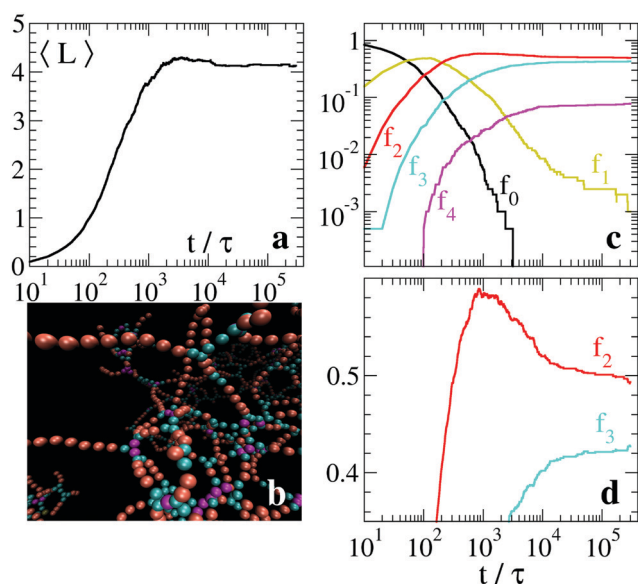

Fig. 6 Relaxation dynamics of a system with N = 2000 particles and λ = 2 for T = 1. (a) Average strand length $\langle L \rangle$. (b) Final configuration of the network: gold, red, cyan, and magenta beads identify, respectively, units with k = 1, 2, 3, 4 contacts. (c) Evolution of the fraction f_k of units with k-contacts in log–log scale and (d) in linear-log scale.

By combining large-scale simulations and analytical estimates of the free energy barriers between motifs, we rationalize the observed slow convergence of the network to equilibrium in terms of the frustrated dynamics of the local motifs. In particular we argue that the relaxation process develops through a sequence of rearrangements that are not only energetically challenging but also require the solution of topological constraints. Importantly, such constraints do not derive from static functional properties of motifs, but emerge dynamically and depend on local thermodynamic conditions. Moreover, the far-from-equilibrium character of our setup is naturally beyond the perturbative regime, where exponential relaxation laws are expected.[7,10]

While we have used a standard temperature quench to produce a clean representation of the network relaxation, in practice the considerations we have drawn should be extended to transient regimes of mechanical or chemical origin. For instance, a passage of a micro-bead through a portion of a viscoelastic fluid made of wormlike micellar networks may "scramble" severely the system by generating dangling ends and by distorting the branches. This unbalanced state then should re-equilibrate by following a relaxation dynamics akin to the one we have characterized here. Such scenario is relevant for microbeads of diameter D traveling with mean velocity v at high Weissenberg number $Wi = v/v_r$, where $v_r = D/\tau_{rel}$ is the velocity scale associated to the relaxation over D with time scale τ_{rel}. Our findings suggest that a proper definition of τ_{rel} should consider the possible emergence of power-law behaviors for strongly disturbed polymer networks. In fact, the relaxation times found here are of the same order of magnitude (seconds) of those measured experimentally in viscoelastic micellar networks.[5,6] It is thus natural to conjecture that τ_{rel} is the time at which each microscopic motif of the network reaches, through a power-law decay, its typical (equilibrium) fraction. In this respect, it is the ending time of this scale-free aging (not to be confused with chemical aging, as a high-temperature degradation of carbon–carbon double bonds[46]) that should be considered for evaluating the standard Deborah and Weissenberg numbers used in experiments.[11,12]

Our findings also raise the question on which of, *e.g.*, self-healing rubber,[47,48] colloidal systems,[49–51] or network fluids[52] do experience a relaxation process characterized by a slow rearrangement of local motifs. In this respect we believe that coarse-grained descriptions based on patchy colloids, as the one presented here, can be highly valuable.

Finally, another perspective of our work is related to the problem of the stability of ring solutions *versus* network structures in self-assembling systems.[24,53] Suitable generalizations of our model could be considered in order to bias the aggregation of linear structures towards the formation of closed rings. For instance, instead of units with two antipodal sticky spots, one could consider patchy particles that are non-axisymmetrically distributed along the surface.[24] The interplay between the branching parameter λ here introduced and the propensity to create rings is an open question that will deserve future investigations.

Conflicts of interest

There are no conflicts to declare.

Appendix

A Numerical methods

Langevin dynamics. Let us consider an ensemble of N patchy particles labeled by the index $i = 1,\ldots,N$ and let $\alpha = 1, 2, 3$ be an additional index that identifies the subunits, where $\alpha = 1$ is the central repulsive core and $\alpha = 2, 3$ identify the two sticky spots in Fig. 1(a). In the following we denote by $\vec{r}_{i\alpha}$ the position of the center of mass of the subunit α of unit i and by $d_{i\alpha}^{j\beta} = |\vec{r}_{i\alpha} - \vec{r}_{j\beta}|$ the distance between two subunits. The repulsive interaction between a pair of central cores of radius R is modeled by a truncated and shifted Lennard-Jones potential

$$U_{LJ}(D_{ij}) = 4\varepsilon\left[\left(\frac{2R}{D_{ij}}\right)^{12} - \left(\frac{2R}{D_{ij}}\right)^6 - \frac{1}{4}\right]\Theta\left(2^{\frac{1}{6}}(2R) - D_{ij}\right), \quad (1)$$

where we have introduced the symbol $D_{ij} = d_{i1}^{j1}$ to simplify the notations. The parameter ε is the typical energy scale of the Lennard-Jones potential and $\Theta(x)$ is the Heaviside function.

The attractive interaction between sticky spots is described by a Gaussian potential with amplitude A and range σ, namely

$$U_G\left(d_{i\alpha}^{j\beta}\right) = -A\,\exp\left[-\left(\frac{d_{i\alpha}^{j\beta}}{\sigma}\right)^2\right], \quad (2)$$

where the subindices α and β are restricted to the values (2,3). Moreover we set

$$\begin{cases} U_{LJ}\left(d_{i\alpha}^{j\beta}\right) = 0 & \text{if } \alpha \text{ or } \beta = (2,3) \\ U_G\left(d_{i\alpha}^{j\beta}\right) = 0 & \text{if } \alpha \text{ or } \beta = 1 \end{cases}. \quad (3)$$

Subunits within each unit evolve as a rigid body arranged as in Fig. 1(a). The evolution of the system is described in terms of a Langevin equation

$$m\frac{d^2\vec{r}_{i\alpha}}{dt^2} = -\gamma\frac{d\vec{r}_{i\alpha}}{dt} - \vec{\nabla}U(\vec{r}_{i\alpha}) + \vec{\eta}_{i\alpha}(t), \quad (4)$$

where $U = U_{LJ} + U_G + $ constraints is the total potential energy function and m is the mass of each subunit. The first term in the r.h.s. of eqn (4) is a linear dissipation proportional to the friction coefficient γ, while $\vec{\eta}_{i\alpha}(t)$ is a Gaussian noise with zero mean and delta-correlated in time. Denoting by $\eta_{i\alpha}^{(\ell)}$ with $\ell = 1, 2, 3$ the Cartesian component of $\vec{\eta}_{i\alpha}$ in the ℓ direction, the noise satisfies a standard fluctuation–dissipation relation in the form

$$\left\langle \eta_{i\alpha}^{(\ell)}(t)\eta_{j\beta}^{(\ell')}(t')\right\rangle = 2\gamma k_B T \delta_{i,j}\delta_{\alpha,\beta}\delta_{\ell,\ell'}\delta(t - t'), \quad (5)$$

where k_B is the Boltzmann constant and T the temperature. Numerical integration of eqn (4) is performed with LAMMPS engine.[36] Nonequilibrium simulations of the system relaxation process are realized according to the following protocol. First we evolve the system described by eqn (4) in the absence of the Gaussian attractive potential ($U_G = 0$) until a uniform

thermalized state is reached. Then we activate U_G and we start monitoring $\langle L \rangle$ and f_k as discussed in the main text.

Physical units. In our simulations the system temperature T is measured in units of ε/k_B, where ε is the amplitude of the Lennard-Jones potential, with $k_B = \varepsilon = 1$, $A = 40\varepsilon$ and $\sigma = 0.4R$. Distances are measured in units of monomer radii R. We set $m/\gamma = \tau$, where $\tau = R\sqrt{m/\varepsilon}$ is the (unitary) characteristic simulation time. In order to estimate the time τ in physical units, one can proceed as follows. From the Stokes formula of the friction coefficient for spherical beads with radius R, we have $\gamma = 6\pi\eta_{sol}R$, where η_{sol} is the viscosity of the solvent. By eliminating m in the above formulas for the characteristic time, one has $\gamma = \varepsilon\tau/(2R)^2$, hence

$$\tau = \frac{3\pi\eta_{sol}(2R)^3}{\varepsilon} \simeq 2 \text{ μs}$$

In the numerical evaluation we consider the nominal water viscosity at room temperature, $\eta_{sol} \simeq 1$ mPa s, and we set $T = \varepsilon/k_B = 300$ K and $R = 5$ nm.

For the large-scale simulations of this work, the system is evolved in a prism of sides $(d,d,3d)$ with $d = 108R$, with periodic boundary conditions. Its volume corresponds to $3d^3 \simeq 0.5$ (μm)^3. If $N = 6000$ units are introduced in this volume, their volume fraction becomes

$$\phi = \frac{N\frac{4}{3}\pi R^3}{3d^3} \simeq 0.7 \times 10^{-2}$$

Contact threshold. Given a configuration of patchy particles identified by the set of $\vec{r}_{i\alpha}$, two distinct units i and $j \neq i$ are considered in contact if there exists a pair of sticky spots α and β such that $d_{i\alpha}^{j\beta} \leq \theta$, where θ is a threshold. To perform an accurate sampling of merging and scission events in the system of particles, θ needs to be of the order of the distance between bound units, in a way that typical thermal fluctuations in their positions of do not produce "spurious" events. To determine a reliable value of θ for the potential U specified in the previous section, we have computed the distributions of sticky spot distances $d_{i\alpha}^{j\beta}$ for all $i \neq j$ in generic networks, see Fig. 8 for an example. The distribution displays a clear gap in the region $[0.5R, 1.8R]$ separating the ensemble of bound sticky spots (with $d_{i\alpha}^{j\beta} \lesssim 0.5R \simeq \sigma$) from the ensemble of unbound ones. Accordingly, we have chosen $\theta = R$, well inside the gap. We have verified that this threshold value is reliable in the whole range of λ and T considered in this work.

Parallel tempering simulations. Free-energy differences between microstates "2" (strands) and "3" (vertices) have been computed through Langevin equilibrium simulations with parallel tempering sampling technique.[39,40] This method is employed to sample accurately the low-temperature equilibrium distribution of the system, thereby reducing the impact of very long correlation times on computational time.

Simulations have been performed for a system of $N = 3$ interacting particles confined in a spherical volume with radius $R_0 = 10.85R$ and volume fraction $\phi \simeq 2 \times 10^{-3}$, which
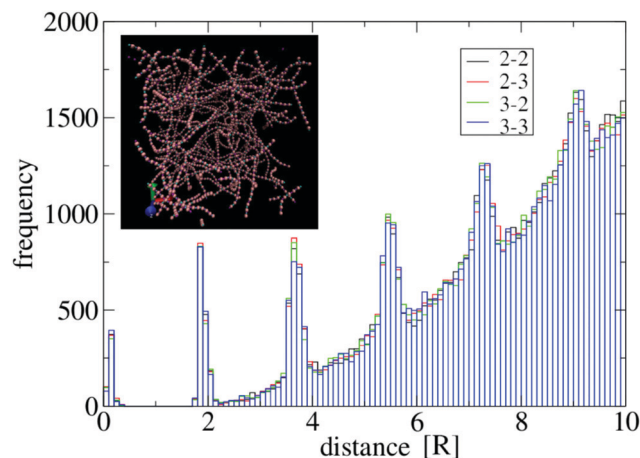
Fig. 8 Distribution of distances between sticky spots for a system of $N = 2000$ particles with $\lambda = 1.75$, $A = 40\varepsilon$ and $\sigma = 0.4R$. Particles are prepared in a homogeneous state and evolved at $T = 1$ according to eqn (4) in a cubic box with side equal to $54R$ and periodic boundary conditions. The histogram is representative of the configuration obtained at $t = 10^5\tau$, see the inset. Black, red, green and blue bars refer respectively to the combination of indices $(\alpha,\beta) = \{(2,2),(2,3),(3,2),(3,3)\}$ in the set of distances $d_{i\alpha}^{j\beta}$ for $i, j = 1,\ldots,N$. Their distributions overlap very well, as expected from symmetry reasons. Multiple peaks above the gap region derive from the regular spacing of particles in the strands.

corresponds to the value of particle density of large-scale simulations with $N = 2000$. We have verified that in this minimal setup the confining volume is sufficiently larger than the typical particle volume, so that it does not introduce significant finite-size effects. The free energy difference ΔF_{32} is computed via the equilibrium Boltzmann distribution $\Delta F_{32} = -T\log(P_3/P_2)$, where P_3 and P_2 are respectively the occupation probabilities of states "3" and "2" sampled over the equilibrium Brownian dynamics. Parallel tempering evolution is performed for a total time of $5 \times 10^6\tau$ with a swapping period of 50τ. Temperature swaps are realized between adjacent temperature states within the set of temperatures considered in Fig. 3(a).

Scission times. Scission times in Fig. 3(b) and (c) have been computed for a system of $N = 3$ interacting particles confined in a spherical volume with radius $R_0 = 10.85R$ and evolving according to eqn (4). For each value of temperature T, particles were initially prepared in a "3" configuration (Fig. 3(b)) and in a "2" configuration (Fig. 3(c)) and evolved until a scission event to a dimer-plus-monomer state (configuration "1") was observed. For each T, the average scission time has been computed by averaging over a sample of 10 independent scission events.

Condensation time scales. Diffusive and ballistic regimes are further analyzed in Fig. 9, where we compare the average particle distance $\bar{d} = \rho_{num}^{-1/3}$ with the typical size $d_c(t)$ of the biggest cluster of particles found in the system at time t. We define $d_c(t) = 2RN_c(t)$, where $N_c(t)$ is the total number of particles in the cluster. We focus on two sizes, namely $N = 25$ (Fig. 9(a)) and $N = 1600$ (Fig. 9(b)), which belong respectively to the diffusive and ballistic condensation regime. For $N = 25$ we
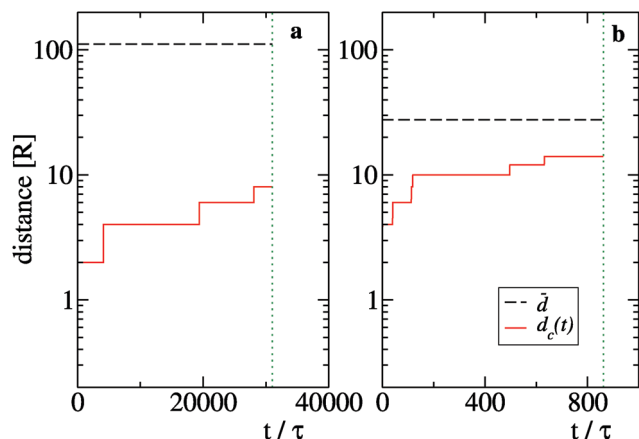
Fig. 9 Evolution of the maximal cluster size $d_c(t)$ (red solid lines) for $N = 25$ (panel (a)) and $N = 1600$ (panel (b)). Black dashed horizontal lines indicate the values of the typical particle distance $\bar{d}$ while green vertical lines identify the time at which f_0 reaches the threshold value f^*.

find $\bar{d} \gg d_c(t)$ during the whole period in which $f_0 > f^*$ while the case $N = 1600$ displays a quick growth of $d_c(t)$ to values which are of the same order of $\bar{d}$ thus suppressing the diffusive scaling of t_0.[45]

Acknowledgements

Notes and references

1 R. G. Weiss and P. Terech, *Molecular Gels*, Springer, Nederlands, 2006.
2 M. Jehser and C. N. Likos, *Colloid Polym. Sci.*, 2020, 1–11.
3 M. E. Cates and S. M. Fielding, *Adv. Phys.*, 2006, **55**, 799–879.
4 R. G. Larson, *The structure and rheology of complex fluids*, Oxford Univesity Press, New York, 1999.
5 J. R. Gomez-Solano and C. Bechinger, *New J. Phys.*, 2015, **17**, 103032.
6 J. Berner, B. Müller, J. R. Gomez-Solano, M. Krüger and C. Bechinger, *Nat. Commun.*, 2018, **9**, 999.
7 M. S. Turner and M. E. Cates, *J. Phys.*, 1990, **51**, 307–316.
8 T. J. Drye and M. E. Cates, *J. Chem. Phys.*, 1992, **96**, 1367.
9 R. Granek and M. E. Cates, *J. Chem. Phys.*, 1992, **96**, 4758.
10 M. S. Turner, C. Marques and M. E. Cates, *Langmuir*, 1993, **9**, 695–701.
11 J. M. Dealy, *Rheol. Bull.*, 2010, **79**, 14–18.
12 R. J. Poole, *Rheol. Bull.*, 2012, **53**, 32–39.
13 J. T. Padding, E. S. Boek and W. J. Briels, *J. Phys.: Condens. Matter*, 2005, **17**, S3347–S3353.
14 J. T. Padding, E. S. Boek and W. J. Briels, *J. Chem. Phys.*, 2008, **129**, 074903.
15 V. Hugouvieux, M. A. V. Axelos and M. Kolb, *Soft Matter*, 2011, **7**, 2580.
16 S. Dhakal and R. Sureshkumar, *J. Chem. Phys.*, 2015, **143**, 024905.
17 P. Wang, S. Pei, M. Wang, Y. Yan, X. Sun and J. Zhang, *J. Colloid Interface Sci.*, 2017, **494**, 47–53.
18 T. Mandal, P. H. Koenig and R. G. Larson, *Phys. Rev. Lett.*, 2018, **121**, 038001.
19 F. Sciortino, C. De Michele, S. Corezzi, J. Russo, E. Zaccarelli and P. Tartaglia, *Soft Matter*, 2009, **5**, 2571–2575.
20 W. Li, H. Palis, R. Mérindol, J. Majimel, S. Ravaine and E. Duguet, *Chem. Soc. Rev.*, 2020, **49**, 1955.
21 D. J. Audus, F. W. Starr and J. F. Douglas, *Soft Matter*, 2018, **14**, 1622–1630.
22 J. Russo, J. Tavares, P. Teixeira, M. T. da Gama and F. Sciortino, *Phys. Rev. Lett.*, 2011, **106**, 085703.
23 J. Russo, J. Tavares, P. Teixeira, M. T. da Gama and F. Sciortino, *J. Chem. Phys.*, 2011, **135**, 034501.
24 L. Rovigatti, J. M. Tavares and F. Sciortino, *Phys. Rev. Lett.*, 2013, **111**, 168302.
25 P. Teixeira and J. Tavares, *Curr. Opin. Colloid Interface Sci.*, 2017, **30**, 16–24.
26 L. Rovigatti, J. Russo and F. Romano, *Eur. Phys. J. E: Soft Matter Biol. Phys.*, 2018, **41**, 59.
27 Q. Chen, S. Chul Bae and S. Granick, *Nature*, 2011, **469**, 381.
28 F. Romano and F. Sciortino, *Soft Matter*, 2011, **7**, 5799.
29 F. Romano and F. Sciortino, *Nat. Mater.*, 2011, **10**, 171.
30 F. Romano and F. Sciortino, *Nat. Commun.*, 2012, **3**, 975.
31 N. A. Mahynski, L. Rovigatti, C. N. Likos and A. Z. Panagiotopoulos, *ACS Nano*, 2016, **10**, 5459–5467.
32 W. F. Reinhart and A. Z. Panagiotopoulos, *J. Chem. Phys.*, 2016, **145**, 094505.
33 H. Eslami, N. Khanjari and F. Mueller-Plathe, *J. Chem. Theory Comput.*, 2019, **15**, 1345–1354.
34 T. Tlusty and S. Safran, *J. Phys.: Condens. Matter*, 2000, **12**, A253.
35 A. Zilman, S. Safran, T. Sottmann and R. Strey, *Langmuir*, 2004, **20**, 2199–2207.
36 S. Plimpton, *J. Comput. Phys.*, 1995, **117**, 1–19.
37 S. Hyde, Z. Blum, T. Landh, S. Lidin, B. Ninham, S. Andersson and K. Larsson, *The language of shape: the role of curvature in condensed matter: physics, chemistry and biology*, Elsevier, 1996.
38 W. Zou, G. Tan, H. Jiang, K. Vogtt, M. Weaver, P. Koenig, G. Beaucage and R. G. Larson, *Soft Matter*, 2019, **15**, 642–655.
39 R. H. Swendsen and J.-S. Wang, *Phys. Rev. Lett.*, 1986, **57**, 2607–2609.
40 M. Tesi, E. J. Van Rensburg, E. Orlandini and S. Whittington, *J. Stat. Phys.*, 1996, **82**, 155–181.
41 K. Vogtt, H. Jiang, G. Beaucage and M. Weaver, *Langmuir*, 2017, **33**, 1872–1880.
42 H. Jiang, K. Vogtt, J. B. Thomas, G. Beaucage and A. Mulderig, *Langmuir*, 2018, **34**, 13956–13964.
43 S. Chandrasekhar, *Rev. Mod. Phys.*, 1943, **15**, 1.
44 G. Carnevale, Y. Pomeau and W. Young, *Phys. Rev. Lett.*, 1990, **64**, 2913.

45 M. S. Veshchunov, *J. Aerosol Sci.*, 2010, **41**, 895–910.

46 Z. Chu, Y. Feng, H. Sun, Z. Li, X. Song, Y. Han and H. Wang, *Soft Matter*, 2011, **7**, 4485.

47 P. Cordier, F. Tournilhac, C. Soulié-Ziakovic and L. Leibler, *Nature*, 2008, **451**, 977.

48 T. F. A. de Greef and E. W. Meijer, *Nature*, 2008, **453**, 171.

49 E. Del Gado and W. Kob, *Europhys. Lett.*, 2005, **72**, 1032–1038.

50 E. Zaccarelli, P. J. Lu, F. Ciulla, D. A. Weitz and F. Sciortino, *J. Phys.: Condens. Matter*, 2008, **20**, 494242.

51 R. Angelini, E. Zaccarelli, F. A. de Melo Marques, M. Sztucki, A. Fluerasu, G. Ruocco and B. Ruzicka, *Nat. Commun.*, 2014, **5**, 4049.

52 C. S. Dias, N. A. M. Araújo and M. M. T. da Gama, *Adv. Colloid Interface Sci.*, 2017, **247**, 258–263.

53 N. G. Almarza, *Phys. Rev. E: Stat., Nonlinear, Soft Matter Phys.*, 2012, **86**, 030101.